

Role of grain boundaries as phonon diffraction gratings in the theory of thermal conductivity

*Original*

Role of grain boundaries as phonon diffraction gratings in the theory of thermal conductivity / Omini, M; Sparavigna, Amelia Carolina. - In: PHYSICAL REVIEW. B, CONDENSED MATTER AND MATERIALS PHYSICS. - ISSN 1550-235X. - 61:(2000), p. 6677. [10.1103/PhysRevB.61.6677]

*Availability:*

This version is available at: 11583/1406029 since: 2021-12-14T09:50:57Z

*Publisher:*

The American Institute of Physics

*Published*

DOI:10.1103/PhysRevB.61.6677

*Terms of use:*

This article is made available under terms and conditions as specified in the corresponding bibliographic description in the repository

*Publisher copyright*

(Article begins on next page)

# Role of grain boundaries as phonon diffraction gratings in the theory of thermal conductivity

M. Omini and A. Sparavigna

*Dipartimento di Fisica and Istituto Nazionale di Fisica della Materia (INFM), Politecnico di Torino,  
C.so Duca degli Abruzzi 24, 10129 Torino, Italy*

(Received 29 July 1999)

The picture of a grain boundary as a periodic array of dislocations implies the occurrence of phonon scattering processes that the Klemens theory of thermal conductivity does not account for. A grain boundary works similar to a diffraction grating, producing diffraction spectra of various orders: each order number  $n$  is associated with a class of scattering processes contributing to thermal resistance. The Klemens theory corresponds to  $n=0$ : it is shown that processes with  $n \neq 0$  are essential to explain the heat transport properties of a specimen containing grain boundaries. The theory is used to explain the behavior of thermal conductivity, both in the range below 5 K and in the region of the conductivity peak, as observed in crystals of lithium fluoride, alumina, and quartz. It is also applied to the conductivity curve of fused silica, in the frame of a model where a glass is pictured as a solid with a high-density distribution of grain boundaries.

## I. INTRODUCTION

The theory of phonon scattering by grain boundaries is still linked to the Klemens formula,<sup>1</sup> which was derived for a wall of edge dislocations. At low temperatures, this formula predicts a thermal resistivity contribution of the form  $AT^{-3}$ , which is typical of boundary scattering. Roth and Anderson<sup>2</sup> (RA) investigated the effect of deformation on the thermal conductivities of some ionic crystals: from their experimental data the change of resistivity due to grain boundary scattering appears to be negligible in the range between 0 K and 4 K. RA considered this result fully consistent with the value of  $A$  deducible from the Klemens formula for sessile grain boundaries.

Recently, Krasavin and Osipov<sup>3</sup> pointed out that the Klemens formula refers to infinitely long walls, while real grain boundaries have a finite length. They simulated finite grain boundaries by wedge disclination dipoles and calculated the phonon relaxation time in the frame of a “potential” approximation similar to that used by Ziman.<sup>4(a)</sup> According to their calculation the thermal conductivity  $\lambda$  of a dielectric solid is such that the product  $\lambda T^{-3}$ , after a marked decrease between 0 and 0.1 K, should exhibit a constant asymptotic value for higher temperatures. The above authors supported this result by making reference to an article of Anderson and Malinowski,<sup>5</sup> who obtained a similar behavior. However, such a behavior was successively denied by RA, after the accurate measurements described in Ref. 2; as a consequence, one is forced to conclude that the model of disclination dipoles is not in agreement with experiment.

We believe the Klemens formula to be unreliable, but not because of the infinitely long wall of dislocations to which it refers: the reason is that it was deduced by neglecting the effect of strain field periodicity on phonon scattering. A periodic wall of edge dislocations works as a diffraction grating: we find that, at temperatures different from absolute zero, diffraction spectra of various orders are called into play, and give rise to a resistivity contribution which is dominant with respect to the one considered by Klemens (zero order).

Owing to such first-principle objection, the results of RA experiments have to be interpreted in terms of a new theory

where the diffraction effects are accounted for. Actually, the discussion of these experiments requires two kinds of explanations, concerning (a) the negligible effect of grain boundaries on thermal conductivity in the range between 0 and 4 K and (b) the deviation of the experimental behavior from the law  $\lambda T^{-3} = \text{const}$ , as observed in the above range for undeformed samples.

Point (b) refers to the fact that according to RA  $\lambda$  increases more slowly than  $T^3$ . We stress that this is a particular case of a general trend which characterizes, in all the crystals, the low-temperature side of the conductivity peak: as a consequence, the peak is never so high as the combination of boundary scattering (giving a resistance contribution proportional to  $T^3$ ) and umklapp scattering would predict. This feature was already emphasized by Berman,<sup>6</sup> who deduced the need for some (unknown) additional scattering mechanism in order to explain the height of the experimental peak in alumina. The theory developed in the present paper suggests a simple explanation in terms of very small angle grain boundaries: a low density distribution of such grain boundaries may be present even in the best grown crystals, and is sufficient to account for the observed behavior in the whole temperature range on the left hand side of the peak.

Finally, the same theory also provides an interesting interpretation of the thermal conductivity curves referring to amorphous dielectric solids. Many scattering mechanisms have been proposed to explain these curves [spatial fluctuation of the sound velocity,<sup>7</sup> resonance scattering from localized phonons,<sup>8</sup> Rayleigh scattering from random displacements of atoms,<sup>9</sup> scattering from localized two level states (TLS's)<sup>10–13</sup>] but all of them are open to objections: the theoretical situation was reviewed by Freeman and Anderson,<sup>14</sup> who concluded that the origin of the observed behavior is unknown. Their criticism is also implicitly directed to theories involving phonon assisted fracton hopping as responsible for an additional contribution to  $\lambda$  in the region above the plateau<sup>15–17</sup>. In fact this contribution turns out to be linear in  $T$ , while Freeman and Anderson point out that a linear dependence is not the dominant feature of the measured thermal conductivity in the above range of temperatures.

We suggest that all the above processes should be considered in the frame of a model where a glass is pictured as a

high-density distribution of random grain boundaries. The reliability of such a description is checked in Sec. VIII, where we discuss, as an example, the inclusion of TLS scattering in the model. We show that in this way it is possible to explain in a satisfactory way the temperature dependence of the conductivity of fused silica between 0.1 and 1 K.

## II. PROBABILITY RATE FOR SCATTERING BY A WALL OF EDGE DISLOCATIONS

To perform a calculation of thermal conductivity, it would be desirable to describe the phonon field by making reference to the true Brillouin zone of the solid: such an approach was actually followed in the simple case of rare gas crystals,<sup>18</sup> and of monoatomic solids with diamond structure,<sup>19</sup> but is expected to present prohibitive difficulties when the unit cell of the crystal contains different kinds of atoms. Since most of the dielectric solids for which the low-temperature behavior of  $\lambda$  has been determined are characterized by a unit cell of this type, we resort to the usual model in which the solid is described as a system of identical atoms, with mass equal to the average atomic mass in the real crystal, the volume of the unit cell being taken as the average volume per atom.<sup>1</sup> Such an approximation, which automatically rules out optical modes, is justified by the fact that these modes are not effective in the low-temperature range in which we are primarily interested.<sup>19</sup> We will further specialize the model by assuming the interaction between atoms to be described by a spherically symmetric pair potential. The model is slightly different from the one discussed by Klemens,<sup>1</sup> but presents the advantage of providing an exact definition of the parameters involved by the phonon scattering matrix element: in fact, for an isotropic solid, these parameters turn out to be all expressible in terms of the Grüneisen constant and of the transverse and longitudinal sound velocities.

In the frame of the above model, the procedure adopted in Ref. 20 allows one to express the matrix element in terms of the displacement field  $\xi_i$  due to any defect present in the lattice: denoting by  $\mathbf{l}$  the position vector running over the  $N_o$  atoms of the perfect crystal, and by  $\delta\xi_{lh} = \xi_{l+h} - \xi_l$  the difference between the displacements of the atoms at  $\mathbf{l}+\mathbf{h}$  and  $\mathbf{l}$ , respectively, one has

$$\begin{aligned} \langle \mathbf{q}', p' | H' | \mathbf{q}, p \rangle = & \frac{\hbar}{4MN_o} \sum_{\mathbf{l}} \sum_{\mathbf{h}} (e^{i\mathbf{q}' \cdot \mathbf{h}} - 1)(e^{-i\mathbf{q} \cdot \mathbf{h}} - 1) \\ & \times e^{i\mathbf{K} \cdot \mathbf{l}} (\omega_{\mathbf{q}}^p \omega_{\mathbf{q}'}^{p'})^{-1/2} \{ A_h(\mathbf{h} \cdot \delta\xi_{lh})(\mathbf{h} \cdot \mathbf{e}_{-\mathbf{q}}^p) \\ & \times (\mathbf{h} \cdot \mathbf{e}_{\mathbf{q}'}^{p'}) + B_h(\mathbf{h} \cdot \delta\xi_{lh})(\mathbf{e}_{-\mathbf{q}}^p \cdot \mathbf{e}_{\mathbf{q}'}^{p'}) \\ & + (\mathbf{h} \cdot \mathbf{e}_{-\mathbf{q}}^p)(\delta\xi_{lh} \cdot \mathbf{e}_{\mathbf{q}'}^{p'}) + (\delta\xi_{lh} \cdot \mathbf{e}_{-\mathbf{q}}^p) \\ & \times (\mathbf{h} \cdot \mathbf{e}_{\mathbf{q}'}^{p'}) \}, \end{aligned} \quad (1)$$

where  $\mathbf{K} = \mathbf{q}' - \mathbf{q}$  and  $M$  is the atomic mass,  $\mathbf{e}_{\mathbf{q}}^p$  the polarization unit vector for a phonon with wave vector  $\mathbf{q}$  and branch index  $p$ ,  $\omega_{\mathbf{q}}^p$  the corresponding angular frequency, while  $A_h, B_h$  denote coupling coefficients containing the derivatives of the pair potential. Equation (1) follows from the expansion of the displacement field in terms of phonon op-

erators, as given by Srivastava:<sup>21</sup> the different representation of the displacement field used in Ref. 20 explains the formal difference between Eq. (1) and the matrix element of the above reference.

We refer to defects for which the displacement field is known from linear elastic theory: this implies the continuum hypothesis and the approximation  $\delta\xi_{lh} = (\partial\xi_l / \partial\mathbf{l}) \cdot \mathbf{h}$ . Consequently the sum over the position vector  $\mathbf{l}$  can be replaced by an integral over the components  $x_1, x_2, x_3$  of this vector and one obtains

$$\sum_{\mathbf{l}} e^{i\mathbf{K} \cdot \mathbf{l}} (\delta\xi_{lh})_k = \frac{N_o}{\Omega} \int d^3x e^{i\mathbf{K} \cdot \mathbf{l}} \frac{\partial\xi_k}{\partial x_j} \mathbf{h}_j, \quad (2)$$

where  $\Omega$  is the volume of the solid and  $\xi_k = [\xi(\mathbf{l})]_k$ . For a defect giving rise to a plane strain (independent of  $x_3 = z$ ) the previous result can be simply written in the form  $2\pi(N_o/\Omega)\delta(K_z)\alpha_{kj}$ , where

$$\alpha_{kj} = \int dx_1 \int dx_2 e^{i(K_1 x_1 + K_2 x_2)} \frac{\partial\xi_k}{\partial x_j}. \quad (3)$$

Since the continuum hypothesis is consistent with the long wavelength approximation, we will write, for any vector  $\mathbf{h}$  whose length is bounded,  $e^{i\mathbf{q} \cdot \mathbf{h}} \simeq 1 + i\mathbf{q} \cdot \mathbf{h}$ : this is precisely the case of the vectors  $\mathbf{h}$  appearing in Eq. (1), because  $A_h, B_h$  are short range functions of the inter-atomic distance, so that  $\mathbf{h}$  is actually confined to the lattice points in the very neighborhood of the atom at the origin. It has to be pointed out that the above approximation becomes a rigorous result in the low temperature limit, where only long wavelength phonons are involved in scattering processes.

In the isotropic model of the solid, the vector  $\mathbf{h}$  is allowed to span with continuity all the directions emerging from the atom which is taken at the origin of the reference frame. The atoms surrounding  $\mathbf{h}=0$  are then assumed to be uniformly distributed over concentric spherical shells of neighbors.<sup>22</sup> If  $s$  is the index labeling a shell with coordination number  $\nu_s$  and radius  $h_s$ , the probability rate concerning the scattering  $\mathbf{q}p \rightarrow \mathbf{q}'p'$ , as deducible from Eq. (1) in the Born approximation, turns out to be expressed in terms of the quantities  $\mathcal{A} = \sum_s \nu_s h_s^6 A(h_s)$ ,  $\mathcal{B} = \sum_s \nu_s h_s^4 B(h_s)$ . The interest of this result lies in the fact that  $\mathcal{A}$  and  $\mathcal{B}$  are directly linked to measurable parameters, namely, the longitudinal and transverse sound velocities  $s_L$  and  $s_T$  and the Grüneisen constant  $\gamma$  [see Eqs. (20) and (22), respectively, of Ref. 22]. Since  $\alpha_{kj}$ , from the dimensional point of view, is an area, it is convenient to put  $\alpha_{kj} = i l_o^2 \beta_{kj}$ , where  $i$  is the imaginary unity and  $l_o^2$  is a reference area in units of which  $\alpha_{kj}$  is measured. Writing  $\delta^2(K_z) = (L_z/2\pi)\delta(K_z)$ , where  $L_z$  is the length of the specimen along  $x_3$ , one finally arrives at the following expression of the probability rate:

$$\begin{aligned} Q_{\mathbf{q}p}^{\mathbf{q}'p'} = & \frac{\pi^2}{4} \frac{q q'}{\Omega^2} \frac{L_z}{s_p s_{p'}} (s_L^2 - s_T^2)^2 l_o^4 |G_{pp'}|^2 \\ & \times \delta(s_{p'} q' - s_p q) \delta(K_z), \end{aligned} \quad (4)$$

where  $G_{pp'}$  is the result of the angular integrations by which we replace the sum over the vectors  $\mathbf{h}$  belonging to a given shell. The integrations are cumbersome but elementary: one obtains

$$G_{pp'}(\beta) = -\frac{\epsilon}{7} T_{ij}^{kl} e_{-\mathbf{q},i}^p e_{\mathbf{q}',j}^{p'} \beta_{kl} + M_{kl} \beta_{kl} e_{-\mathbf{q},i}^p e_{\mathbf{q}',i}^{p'} + M_{ik} \beta_{jk} [e_{-\mathbf{q},i}^p e_{\mathbf{q}',j}^{p'} + e_{-\mathbf{q},j}^p e_{\mathbf{q}',i}^{p'}], \quad (5)$$

where  $\epsilon = -\mathcal{A}/B$  and the tensors  $T_{ij}^{kl}, M_{kl}$  are defined in terms of the couples of angles  $(\theta, \phi)$  and  $(\theta', \phi')$  specifying the directions of  $\boldsymbol{\mu}_q = \mathbf{q}/q$  and  $\boldsymbol{\mu}_{q'} = \mathbf{q}'/q'$ , respectively (see the Appendix). The same angles enter the expressions of the polarization vectors required by Eq. (5). In the isotropic model  $\mathbf{e}_q^3$  (polarization vector of the longitudinal branch) is parallel to  $\mathbf{q}$ , and coincident with  $\boldsymbol{\mu}_q = \sin \theta \cos \phi \mathbf{i} + \sin \theta \sin \phi \mathbf{j} + \cos \theta \mathbf{k}$ , where  $\mathbf{i}, \mathbf{j}, \mathbf{k}$  are the unit vectors of the axes  $x_1, x_2, x_3$ . The vector  $\mathbf{e}_q^2$  can be chosen in any direction normal to  $\mathbf{e}_q^3$ : the most convenient choice is  $\mathbf{e}_q^2 = \sin \phi \mathbf{i} - \cos \phi \mathbf{j}$ , and consequently  $\mathbf{e}_q^1 = -\cos \theta \cos \phi \mathbf{i} - \cos \theta \sin \phi \mathbf{j} + \sin \theta \mathbf{k}$ .

Let us refer to a parallelepiped sample, with sides parallel to the three coordinate axes  $x_1, x_2, x_3$  and corresponding lengths  $L_x, L_y, L_z$ . Let it contain a symmetric tilt boundary, that, according to Hirth and Lothe (HL),<sup>23</sup> we model as a periodic array of  $N$  edge dislocations distributed with spacing  $D$  along the  $y = x_2$  axis: all the dislocations have Burger vector  $b$  and axis parallel to  $z = x_3$ . The origin of the reference frame is taken at the center of the parallelepiped, and assumed to lie on the axis of one of the  $N$  dislocations. In this case it is convenient to choose  $l_o^2 = bD$ . Since the tensor  $\xi_{kj}(x, y) = \partial \xi_k / \partial x_j$  is such that  $\xi_{kj}(x, y + pD) = \xi_{kj}(x, y)$  for any integer value of  $p$ , it is easy to deduce from Eq. (3)

$$\begin{aligned} \beta_{kj} &= \exp \left[ -i \frac{K_y(N-1)D}{2} \right] \{ 1 + e^{iK_y D} + e^{i2K_y D} + \dots \} \tau_{kj} \\ &= \exp \left( -\frac{iNK_y D}{2} \right) \frac{\sin[(N-1)K_y D/2]}{\sin(K_y D/2)} \tau_{kj}, \end{aligned} \quad (6)$$

where the last step follows from an explicit evaluation of the curly bracket, which contains  $N-1$  terms and

$$\tau_{kj} = \frac{1}{ibD} \int_0^D dy e^{iK_y y} \int_{-L_x/2}^{L_x/2} dx e^{iK_x x} \xi_{kj}(x, y). \quad (7)$$

Since  $N$  is very large,  $\beta_{kj}$  is significantly different from zero only for values of  $K_y$  satisfying the condition

$$\frac{K_y D}{2} = n\pi, \quad (8)$$

where  $n$  is any integer. In this case one has simply

$$l_o^4 |G_{pp'}|^2 = b^2 N^2 D^2 |F_{pp'}|^2 = b^2 L_y^2 |F_{pp'}|^2, \quad (9)$$

where  $F_{pp'}$  is the expression obtainable from Eq. (5) by substituting the tensor  $\tau_{kj}$  to the tensor  $\beta_{kj}$ . The expressions of  $\tau_{kj}$  are easily evaluated by the use of the displacement field and of the stress components appropriate to the symmetric tilt boundary, as given, for instance, by HL (pp. 78

and 732 of Ref. 23). Particular care has to be taken in writing the expressions of  $\tau_{12}$  and  $\tau_{21}$ . The former turns out to be

$$\begin{aligned} \tau_{12} &= \frac{1}{D^2} \int_0^D dy \cos(K_y y) \int_0^{L_x/2} dx \sin(K_x x) \left[ \frac{\sinh 2\pi X}{C} \right. \\ &\quad \left. + \frac{\pi}{1-\nu} \frac{X(\cosh 2\pi X \cos 2\pi Y - 1)}{C^2} \right], \end{aligned} \quad (10)$$

where  $X = x/D, Y = y/D$  and  $C = C(X, Y) = \cosh 2\pi X - \cos 2\pi Y$ . It is convenient to add and subtract a unity inside the square bracket. The term  $-1$ , when added to the argument of the bracket, gives rise to a function which strongly decreases for large values of  $x$  and, consequently, to an integral which can be extended from  $x=0$  to  $x=\infty$ . Conversely, the remaining term  $+1$  engenders the integral

$$\tau^* = \frac{1}{D^2} \int_0^D dy \cos(K_y y) \int_0^{L_x/2} \sin(K_x x) dx \quad (11)$$

which depends on the length  $L_x$  of the specimen. Owing to Eq. (8)  $\tau^*$  is different from zero only for  $K_y = 0$ . In this case it is given by  $[1 - \cos(K_x L_x/2)]/K_x D$ . Since, however, because of the periodicity conditions imposed to the phonon states,  $K_x = 2m\pi/L_x$ , where  $m$  is an integer, one can also write

$$\tau^*(K_x D) = \delta_{n,0} \frac{1 - (-1)^m}{K_x D}. \quad (12)$$

An analogous procedure can be used for the evaluation of  $\tau_{21}$ , while it is not required for  $\tau_{11}$  and  $\tau_{22}$ : in fact the corresponding integrands are strongly decreasing for  $x \rightarrow \infty$ . The final result can be expressed in the form  $\tau_{kj} = 0$  for  $k=3$  or  $j=3$ , and  $\tau_{kj} = g_{kj}(K_x D)$ , for  $k=1$  or  $2, j=1$  or  $2$ , where the functions  $g_{kj}(\eta)$  are defined as  $g_{11}(\eta) = f_+(\eta)$ ,  $g_{22}(\eta) = f_-(\eta)$ ,  $g_{12}(\eta) = g_+(\eta)$ ,  $g_{21}(\eta) = g_-(\eta)$ , with

$$\begin{aligned} f_{\pm}(\eta) &= -\frac{1}{2(1-\nu)} \int_0^1 dY \sin 2n\pi Y \\ &\quad \times \int_0^\infty dX \frac{\cos \eta X \sin 2\pi Y}{C^2} \\ &\quad \times [(1-2\nu)C \pm 2\pi X \sinh 2\pi X] \end{aligned} \quad (13)$$

$$\begin{aligned} g_{\pm}(\eta) &= \int_0^1 dY \cos 2n\pi Y \int_0^\infty dX \sin \eta X \left\{ \pm \frac{\sinh 2\pi X}{C} + 1 \right. \\ &\quad \left. + \frac{\pi X}{1-\nu} \frac{\cosh 2\pi X \cos 2\pi Y - 1}{C^2} \right\} \pm \tau^*(\eta). \end{aligned} \quad (14)$$

### III. PHONON TRANSPORT EQUATION

The Boltzmann equation for the phonon distribution  $n_q^p$  can be written in terms of the deviation function  $\Phi_q^p$  defined by the relation  $n_q^p = \bar{n}_q^p + (k_B T)^{-1} \bar{n}_q^p (1 + \bar{n}_q^p) \Phi_q^p$ , where  $\bar{n}_q^p$  is the Bose-Einstein distribution. The linearized Boltzmann equation is

$$s_q^p \frac{\partial \bar{n}_q^p}{\partial T} \nabla T = \frac{1}{k_B T} \sum_{q'} \bar{n}_q^p (1 + \bar{n}_q^p) \mathcal{Q}_{qp}^{q'p'} (\Phi_{q'}^{p'} - \Phi_q^p) - \frac{\bar{n}_q^p (1 + \bar{n}_q^p)}{k_B T} \frac{\Phi_q^p}{\tau_q^p}, \quad (15)$$

where  $s_q^p = s_p \mu_q$  is the phonon velocity and  $\tau_q^p$  is the relaxation time for boundary scattering.

A tilt boundary similar to that previously described is composed by an array of dislocations with axis parallel to  $z$ , and piled up along the  $y$  axis. It will be denoted by the symbol  $[z, y]$ . It is interesting to discuss a model where grain boundaries with planes normal to  $x, y$  and to  $z$  coexist in our parallelepiped specimen. This model is analogous to that treated by Ziman,<sup>4(b)</sup> for a solid containing three sets of dislocation lines parallel to the coordinate axes. Since a tilt boundary with plane normal to  $x$  can be represented either by  $[z, y]$  or by  $[y, z]$ , etc., it follows that in the above model the specimen contains dislocation arrays of all the following forms:

$$[z, y], [y, z], [x, z], [z, x], [y, x], [x, y]. \quad (16)$$

Let  $N'_x, N''_x, N'_y, N''_y, N'_z, N''_z$  be their corresponding numbers. We will first evaluate the contribution to the first term on the right hand side of Eq. (15) by the  $N'_x$  tilt boundaries of the form  $[z, y]$ . We use the substitution

$$\sum_{q'} \rightarrow (2\pi)^{-2} L_x L_z \int dq'_x \int dq'_z \sum_n \quad (17)$$

to obtain for the above contribution the expression

$$\frac{\bar{n}_q^p (1 + \bar{n}_q^p)}{k_B T} \frac{1}{16} b^2 \frac{N'_x}{L_x} (s_L^2 - s_T^2)^2 q^2 \times \sum_{p'} \frac{s_p}{s_{p'}^4} \sum_n \sum_j \left\{ \frac{|F_{pp'}|^2}{|\gamma_{pp'}^{nj}|} (\Phi_{q'}^{p'} - \Phi_q^p) \right\}_{q' = q'^j_n}. \quad (18)$$

This has been deduced on account of Eqs. (4) and (9) and of the relation  $\Omega = L_x L_y L_z$ . We have put  $\gamma_{pp'}^{nj} = q_{pp',n}^j / q$ , where

$$q_{pp',n}^j = \pm \left[ \left( \frac{s_p}{s_{p'}} \right)^2 q^2 - \left( q_y + \frac{2n\pi}{D} \right)^2 - q_z^2 \right]^{1/2} \quad (19)$$

and the index  $j$  labels the two possible choices of sign. The vector denoted by  $\mathbf{q}_n^{j,j}$  has components  $q_{pp',n}^j, q_y + 2n\pi/D, q_z$ : correspondingly, the argument of functions  $g_{ki}$  is  $K_x D = (q_{pp',n}^j - q_x) D$ .

To deduce Eq. (18), any interference effect between different scatterers has been neglected: this assumption is reasonable if the distribution of scatterers is random, that is if the distance between adjacent tilt boundaries of the set is a random variable.

Through suitable substitutions, expression (18) can be used to obtain the contribution of the other tilt boundaries. For instance, in the case of the  $N'_y$  tilt boundaries of the form  $[x, z]$ , one has simply to change  $N'_x/L_x$  into  $N'_y/L_y$  and impose the scattering conditions  $q'_x = q_x, q'_z = q_z$

+  $2n\pi/D, s_{p'}, q' = s_p q$ . The nonvanishing components of  $\tau_{kj}$  turn out to be in this case  $\tau_{22}, \tau_{33}, \tau_{23}$ , and  $\tau_{32}$ . Therefore, one obtains the appropriate form of  $F_{pp'}$  by retaining in  $G_{pp'}(\tau)$  only the terms proportional to the above quantities, which are now represented by  $\tau_{22} = g_{11}(K_y D)$ ,  $\tau_{33} = g_{22}(K_y D)$ ,  $\tau_{23} = g_{12}(K_y D)$ ,  $\tau_{32} = g_{21}(K_y D)$ . The quantity  $\gamma_{pp'}^{nj}$  is now defined as  $q'_y/q$ , where  $q'_y$  follows from the scattering conditions.

We note that  $N_x/L_x = (N'_x + N''_x)/L_x$  is the linear density of grain boundaries with plane normal to the  $x$  axis. Assuming  $N'_x = N''_x$  and  $N_x/L_x = N_y/L_y = N_z/L_z = \mathcal{N}$ , one easily obtains the final expression for the first term on the right-hand side (RHS) of Eq. (15). It is of the form (18), where  $N'_x/L_x$  is substituted by  $\mathcal{N}/2$ , and the curly bracket by a sum over the values taken by the bracket for each of the six dislocation arrays (16). Since the three axes are treated in the same way, the model represents a satisfactory approximation for a solid containing grain boundaries without a preferential orientation.

At this point, it is possible to write the Boltzmann equation for a sample containing all the dislocation arrays. To this purpose, it is convenient to introduce the dimensionless variable  $t = \hbar s_T q / k_B T$  and put the deviation function in the form

$$\Phi_q^p = \frac{32\hbar^2 s_T^6}{b^2 (s_L^2 - s_T^2)^2 \mathcal{N} k_B T^2} \frac{1}{t} \sum_i f_i^p(t, \theta, \phi) \frac{\partial T}{\partial x_i}. \quad (20)$$

The transport equation is then

$$\frac{s_p}{s_T} \mu_i(t, \theta, \phi) = \sum_{p'}^* \left( \frac{s_T}{s_{p'}} \right)^4 \sum_{n=-\infty}^{+\infty} \sum_{\sigma=1}^6 \sum_j \left\{ \frac{|F_{pp'}|^2}{|\gamma_{pp'}^{nj}|} \times \left[ \frac{s_{p'}}{s_p} f_i^{p'}(t', \theta', \phi') - f_i^p(t, \theta, \phi) \right] \right\}_{\sigma} - \frac{\rho}{t^2} f_i^p(t, \theta, \phi), \quad (21)$$

where

$$\rho = \frac{32\hbar^2 s_T^2}{\mathcal{N} b^2 \mathcal{L} k_B^2 T^2} \frac{s_T^4}{(s_L^2 - s_T^2)^2}, \quad (22)$$

$\mathcal{L} = s_p \tau_q^p$  being the Casimir length for boundary scattering. The index  $\sigma$  in Eq. (21) specifies the particular dislocation array for which the curly bracket must be calculated: the values 1,2,3,4,5,6 of this index will be used to denote the arrays listed in Eq. (16).

The asterisk in Eq. (21) recalls that, for a given  $t$ , the sum involves only the branches for which the wavelength  $\mathbf{q}'$  of the emerging phonon satisfies the condition  $q' \leq Q$ , where  $Q$  is the radius of the Debye sphere: such a condition can be written  $(s_p/s_{p'})t \leq \Theta/T$ , where  $\Theta = \hbar s_T Q / k_B$  plays the role of a characteristic temperature, different in principle from the Debye temperature  $\Theta_D$ .



TABLE I. Expression of the quantities required to describe the phonon scattering process  $\mu \equiv (\mu_\alpha, \mu_\beta, \mu_\gamma) \rightarrow \mu' \equiv (\mu'_\alpha, \mu'_\beta, \mu'_\gamma)$ , as produced by a dislocation wall  $[x_\alpha, x_\beta]$ .

$\mu'_\alpha$	$\mu'_\beta$	$\mu'_\gamma$	$\gamma_{pp'}^{nj}$	$\psi_{pp'}$
$\frac{s_{p'}}{s_p} \mu_\alpha$	$\frac{s_{p'}}{s_p} \left( \mu_\beta + \frac{2n\pi}{\chi t} \right)$	$\frac{s_{p'}}{s_p} \gamma_{pp'}^{nj}$	$\pm \left[ \left( \frac{s_p}{s_{p'}} \right)^2 - \mu_\alpha^2 - \left( \mu_\beta + \frac{2n\pi}{\chi t} \right)^2 \right]^{1/2}$	$\chi [\gamma_{pp'}^{nj} - \mu_\gamma]$

Each curly bracket of Eq. (21) requires the expressions of  $t', \theta', \phi'$  in terms of  $t, \theta, \phi$ . First of all, owing to the energy conservation equation in the scattering process, one has  $t' = s_p t / s_{p'}$ . Moreover, we recall that  $\theta, \phi$  define the direction  $\mu = \mathbf{q}/q$  of the incoming phonon, and  $\theta', \phi'$ , the direction  $\mu' = \mathbf{q}'/q'$  of the scattered phonon. If  $\sigma$  refers to the dislocation array  $[x_\alpha, x_\beta]$ , the expressions of  $\theta', \phi'$  in terms of  $\theta, \phi$ , though not explicitly written, are easily obtained through the relations between the components of  $\mu'$  and  $\mu$  as given in Table I, where the axis denoted by  $\gamma$  is normal to the axes denoted by  $\alpha$  and  $\beta$ . The corresponding nonvanishing components of  $\tau_{jk}$  are  $\tau_{\gamma\gamma} = g_{11}$ ,  $\tau_{\beta\gamma} = g_{21}$ ,  $\tau_{\gamma\beta} = g_{12}$ ,  $\tau_{\beta\beta} = g_{22}$ : the argument of functions  $g_{jk}$  (that is,  $K_x D$  for  $\sigma = 1, 2$ ;  $K_y D$  for  $\sigma = 3, 4$ ;  $K_z D$  for  $\sigma = 5, 6$ ) can be generally written as  $\psi_{pp'} t$ , where  $\Psi_{pp'}$  is given by the last column of the table, and  $\chi$  is the dimensionless parameter

$$\chi = \frac{k_b T D}{\hbar s_T}. \quad (23)$$

Particular care is required to handle the term on the (RHS) of Eq. (21) with  $n=0$ . In such a case  $F_{pp'}$  contains the function defined by Eq. (12), which can be written as  $\tau^* = \xi_m / \lambda_m$ , where  $\xi_m = 1 - (-1)^m$  and  $\lambda_m = 2m\pi D / L_\alpha$  for a set of grain boundary planes normal to the parallelepiped side with length  $L_\alpha$ . Correspondingly one has  $F_{pp'} = F_{pp'}^o + \xi_m H_{pp'} / \lambda_m$ , where  $F_{pp'}^o$  is the expression deducible from  $F_{pp'}$  when  $\tau^*$  in Eqs. (13), (14) is omitted, while  $H_{pp'}$ , for the dislocation array  $[x_\alpha, x_\beta]$ , is represented by

$$H_{pp'} = -M_{i\gamma} [e_{-\mathbf{q},i}^p e_{\mathbf{q}',\beta}^{p'} + e_{-\mathbf{q},\beta}^p e_{\mathbf{q}',i}^{p'}] + M_{i\beta} [e_{-\mathbf{q},i}^p e_{\mathbf{q}',\gamma}^{p'} + e_{-\mathbf{q},\gamma}^p e_{\mathbf{q}',i}^{p'}]. \quad (24)$$

Owing to the invariance of  $T_{ij}^{kl}$  and  $M_{kl}$  with respect to the exchange  $k \rightleftharpoons l$ , the first and second term on the RHS of Eq. (5) contain  $\tau_{12}$  and  $\tau_{21}$  only through the combination  $\tau_{12} + \tau_{21}$ , which is independent of  $\tau^*$ . Thus the dependence of  $F_{pp'}$  on  $\tau^*$  originates from the third term of Eq. (5), which precisely leads to Eq. (24). One readily obtains

$$|F_{pp'}|^2 = |F_{pp'}^o|^2 + \Lambda_{pp'}, \quad (25)$$

where

$$\Lambda_{pp'} = 4 \left[ \left( \frac{H_{pp'}}{\lambda_m} \right)^2 + F_{pp'}^o \frac{H_{pp'}}{\lambda_m} \right] \quad (m \text{ odd}), \quad (26)$$

$$\Lambda_{pp'} = 0 \quad (m \text{ even}). \quad (27)$$

Equation (27) also holds for  $m=0$  (i.e.,  $\lambda_m=0$ ), consistently with the limit of Eq. (11) for  $K_x \rightarrow 0$ . Considering that

in this case also  $F_{pp'}^o$  vanishes [as shown by the integrals of Eqs. (13), (14) evaluated for  $n=0, \eta=0$ ], one has  $|F_{pp'}|^2 = 0$ , so that for  $n=0$  the probability rate is zero for all the processes for which the argument of functions  $g_{kj}$  is zero. In particular, this rules out the value of  $j$  leading to  $\psi_{pp'} = 0$  in processes with  $n=0$  and  $s_p = s_{p'}$ . The final expression of the conductivity will contain a sum over all the possible values of  $\lambda_m$ : when the size of the specimen is large,  $\lambda_m$  spans a continuum, and the only reasonable approximation to evaluate the above sum consists in assigning to  $\Lambda_{pp'}$ , the average of the two values (26) and (27), namely

$$\Lambda_{pp'} = 2 \left[ \left( \frac{H_{pp'}}{\psi_{pp'} t} \right)^2 + F_{pp'}^o \frac{H_{pp'}}{\psi_{pp'} t} \right]. \quad (28)$$

We emphasize that this term is called into play only for processes with  $n=0$ . When  $n \neq 0$  Eq. (25) holds with  $\Lambda_{pp'} = 0$ .

#### IV. SOLUTION OF THE TRANSPORT EQUATION AND THERMAL CONDUCTIVITY

The transport equation (21) will be solved through an iteration procedure, already employed in previous works.<sup>18,19</sup> To generate the zero-order solution, one neglects the term containing  $f_i^{p'}(t', \theta', \phi')$ : the first order solution is obtained by substituting into the same term the zero-order solution, and so on. If the procedure is convergent, the limit for  $k \rightarrow \infty$  of the  $k$ th order solution represents the rigorous solution of the transport equation. Once  $f_i^p$  is obtained, the thermal current density  $\mathbf{U}$  can be calculated. From its expression

$$\mathbf{U} = \frac{1}{k_B T \Omega} \sum_{\mathbf{q}} \hbar s_p q s_{p'} \mu_q \bar{n}_{\mathbf{q}p'} (1 + \bar{n}_{\mathbf{q}p'}) \Phi_{\mathbf{q}p'} \quad (29)$$

and from Eq. (20) one readily deduces  $U_n = -\sum_i \lambda_{ni} \partial T / \partial x_i$ , where the conductivity tensor  $\lambda_{ni}$  is given by

$$\lambda_{ni} = -k_o \sum_p \left( \frac{s_p}{s_T} \right)^2 \int_0^{\Theta/T} t^2 \bar{n}_p (1 + \bar{n}_p) dt \int_0^\pi \sin \theta d\theta \times \int_0^{2\pi} d\phi \mu_n(\theta, \phi) f_i^p(t, \theta, \phi) \quad (30)$$

the quantity  $k_o$  being defined as

$$k_o = \frac{4}{\pi^3} \frac{s_T^4}{(s_L^2 - s_T^2)^2} \frac{k_B^2 T}{\hbar b^2 \mathcal{N}} \quad (31)$$

while  $\bar{n}_p = [\exp(s_p t / s_T) - 1]^{-1}$ . Let us discuss the limiting behavior of the conductivity for  $T \rightarrow 0$ . In this limit, since the

arguments  $\Psi_{pp',t}$  of functions  $g_{kj}$  are proportional to  $T$  [see Eq. (23) and Table I], one deduces from Eqs. (13), (14) that the dominant contribution to  $g_{12}$  and  $g_{21}$  is from the term  $\tau^*$ . On the other hand, when the temperature is very low, for any  $n \neq 0$  the argument of the square root defining  $\gamma_{pp'}^{nj}$  is highly negative (see the fourth column of Table I), so that only for  $n=0$  one finds a real value of  $\gamma_{pp'}^{nj}$ . Thus in the above limit  $g_{11}$  and  $g_{22}$  vanish. One deduces that  $F_{pp'}^o$  vanishes and consequently from Eq. (28)

$$|F_{pp'}|^2 = 2 \left| \frac{H_{pp'}}{\Psi_{pp'}} \right|^2 \frac{1}{t^2}. \quad (32)$$

Substituting this expression into Eq. (21) one notes that  $|F_{pp'}|^2$  and the boundary scattering term have the same  $t$  dependence ( $\propto 1/t^2$ ): moreover, since  $\psi_{pp'}$  is proportional to  $\chi$ , they turn out to have also the same temperature dependence ( $\propto 1/T^2$ ). Consequently, if one defines the function  $F_i^p = f_i^p / \chi^2 t^2$ , one finds for  $F_i^p$  an equation where any dependence on  $t$  and  $T$  disappears. This means that  $f_i^p$  can be put in the form  $\chi^2 t^2 F_i^p$ , where  $F_i^p$  depends only on the angular coordinates. When such a form is substituted into Eqs. (30), (31), the conductivity tensor becomes proportional to  $k_o \chi^2$ , and therefore to  $T^3$ .

We also note that in the above case, the conductivity turns out to be expressible in terms of harmonic quantities such as the sound velocities. This is a consequence of the central potential model, which allows the anharmonic Hamiltonian [and consequently the matrix element (1)] to be split into two parts, one of them being characterized by the same coefficient  $B_h$  appearing in the expression of the Hamiltonian for the harmonic phonon system.<sup>22,24</sup> Since the quantity  $H_{pp'}$  contained in Eq. (32) is due to the last term of Eq. (5), which in turn derives only from the part of the matrix element (1) proportional to  $B_h$ , there is no surprise that the corresponding contribution to thermal conductivity can be expressed in terms of purely harmonic parameters.

Looking now at the expression of  $\gamma_{pp'}^{nj}$  in Table I, one sees that the ratio  $2\pi n / \chi t$  must not be too high, in order to warrant the reality of  $\gamma_{pp'}^{nj}$ . It must not exceed a value depending on the angular coordinates, but anyway of the order of unity. Owing to Eq. (23), this means

$$t > \sim \frac{2\pi \hbar s_T n}{k_B T D}. \quad (33)$$

For a given value of the order number  $n$ , such a condition implies, in the very low-temperature limit, very large values of  $t$ , whose contribution, however, is heavily damped by the exponential in the Bose-Einstein function. Thus for  $T \rightarrow 0$  processes with  $n \neq 0$  are not effective. However, their weight can be increased by raising the temperature of the specimen, because in this way the values of  $t$  required to satisfy Eq. (33) are reduced. To perform the numerical analysis, one fixes an integer  $n_o \neq 0$  and solves the transport equation (21) by confining the sum over  $n$  to the range  $-n_o \leq n \leq n_o$ : consequently, one calculates through Eq. (30) a conductivity depending on the choice of  $n_o$ . A plot of  $\lambda_{ni}(n_o)$  as a function of  $n_o$  shows the value of  $n_o$  to be chosen in order to arrive at a satisfactory convergence. Another problem concerns the

convergence of the iteration procedure employed to solve the transport equation. The convergence can easily be checked by plotting the conductivity as a function of the maximum order of iteration ( $i_{\max}$ ) adopted in the numerical solution of Eq. (21). The results of our numerical analysis show that for  $n_o = 5$  and  $i_{\max} = 20$  the convergence of the sum over  $n$  and of the iteration procedure are both warranted in the whole temperature range.

## V. COMPARISON WITH KLEMENS THEORY

In studying the scattering produced by a wall of edge dislocations, piled up with spacing  $D$  along the  $y$  axis, Klemens<sup>1</sup> neglected the periodic dependence on  $y$  of the strain field. In fact he approximated by an integral the sum over the dislocations of the wall, obtaining a field  $\partial \xi_k / \partial x_j$  depending only on the  $x$  variable. The consequence of this approximation is that the scattering matrix element, being proportional to Eq. (3), contains a factor  $\delta(K_y)$ : in other words, only scattering processes for which  $K_y = 0$  are allowed. This situation corresponds to putting  $n=0$  in Eq. (8): consequently  $g_{11} = g_{22} = 0$ , and  $g_{12} \approx -g_{21} \approx \tau^*$ , since the integrals appearing in Eqs. (13) and (14) turn out to be always negligible, for  $n=0$ , with respect to  $\tau^*$ . Thus Eq. (32) holds, and the conclusions are precisely the ones written as a comment to the above equation: the conductivity is proportional to  $k_o \chi^2$ , namely, to  $T^3 D^2$ , in full agreement with the expression of the relaxation time given by Klemens. We point out that the particular dependence on  $D$  implies that the thermal resistance vanishes for  $D \rightarrow \infty$ , that is for small misfit angles  $\theta = b/D$ .

Deviations from Klemens' theory, and therefore from the above conclusions, are connected to values of  $n$  different from zero. These terms are sensitive to the periodic structure of the grain boundary, which is concealed in the integrals appearing in Eqs. (13), (14). In a paradoxical way, they give rise to a thermal resistance which increases with  $D$ , that is becomes larger for smaller values of the misfit angle. The basic reason of this result lies in the fact that for a wall of edge dislocations with axis parallel to  $z$  and piled up along  $y$ , the strain field is approximately confined to the slab  $|x| \leq \sim D$  (Ref. 23 p. 741): consequently, by reducing  $\theta$  (increasing  $D$ ) the volume fraction affected by the field is increased and the scattering power of the wall becomes more relevant. Of course, this conclusion holds provided we are dealing with a periodic wall: for a specimen with a finite side along  $y$  (that is, for a finite value of  $L_y$ ) such a condition is verified if we neglect the departure from periodicity due to the dislocations of the wall lying in proximity of the boundaries. The approximation is reasonable if the number  $N$  of dislocations forming the wall is high, therefore if  $L_y/D \gg 1$  or

$$\theta \gg b/L_y. \quad (34)$$

For all the values of  $\theta$  satisfying Eq. (34) the theory developed in the previous section can be applied and the grain boundary contribution  $R$  to the thermal resistance is expected to increase by a reduction of the misfit angle. On the other hand, a rigorous theory accounting for the departure from periodicity would obviously lead to a vanishing thermal resistance for  $\theta \rightarrow 0$  (absence of dislocations in the wall): as a result, the curve  $R(\theta)$  is expected to present a maximum. We

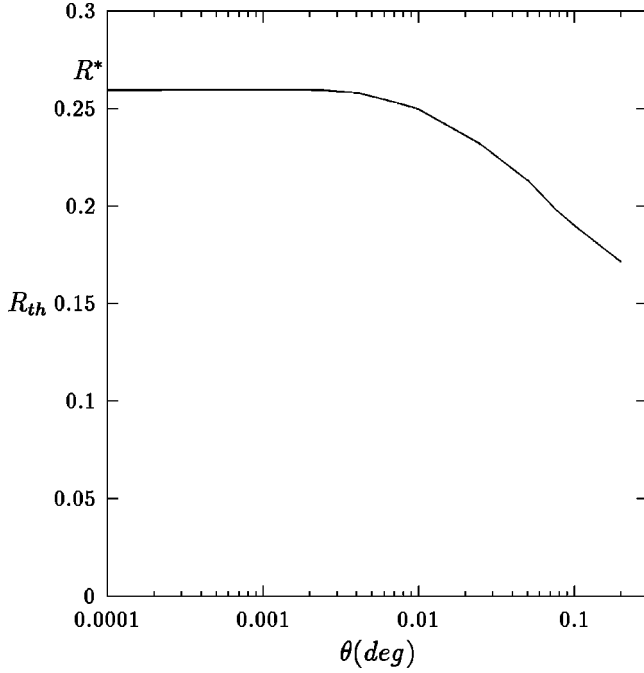


FIG. 1. Thermal resistance [ $R = 1/\lambda$  in units of (cm K)/W] for a specimen of LiF at 5 K as a function of the grain boundary misfit angle  $\theta$ .

will always work in the region on the right hand side of the maximum, where Eq. (34) is satisfied, and our theoretical curve  $R_{th}(\theta)$ , shows the behavior sketched in Fig. 1. The extrapolation of  $R_{th}$  for  $\theta \rightarrow 0$  leads to a saturation value, say  $R^*$ , which is obviously unphysical: however, the form of such asymptotic behavior ensures that in the range where Eq. (34) is satisfied (and nevertheless  $\theta$  is small) the contribution to thermal resistance is weakly depending on  $\theta$ , so that  $R^*$  can be adopted as the representative resistance of very low angle grain boundaries of physical interest.

In the light of the present theory, which role is left to processes with  $n = 0$  (the only ones considered by Klemens)? They are obviously effective only in the very neighborhood of absolute zero. However, also in this case, if the density of grain boundaries is small (see Secs. VI and VII), their contribution to thermal resistance is negligible, being swamped by the more relevant contribution of boundary scattering. The result is that for  $T \rightarrow 0$  the value of  $\lambda$  is essentially determined by the Casimir length  $\mathcal{L}$ , through the formula

$$(\lambda T^{-3})_{T \rightarrow 0} = \frac{2\pi^2}{45} \frac{k_B^4}{\hbar^3} \mathcal{L} \left( \frac{2}{s_T^2} + \frac{1}{s_L^2} \right) \quad (35)$$

which can easily be found by investigating the limit for  $\mathcal{N} \rightarrow 0$  of the present theory or, more directly, extending Callaway's calculation<sup>25</sup> to a model where the distinction between longitudinal and transverse sound velocities is allowed. In this way Eq. (35) can be used to obtain  $\mathcal{L}$  from the experimental limit of  $\lambda T^{-3}$ . Things go differently when  $\mathcal{N}$  is high, as in amorphous solids (Sec. VIII): in such a case the above limit is heavily affected by the presence of grain boundaries and cannot be used to determine  $\mathcal{L}$ , which is approximately taken as the size of the sample.

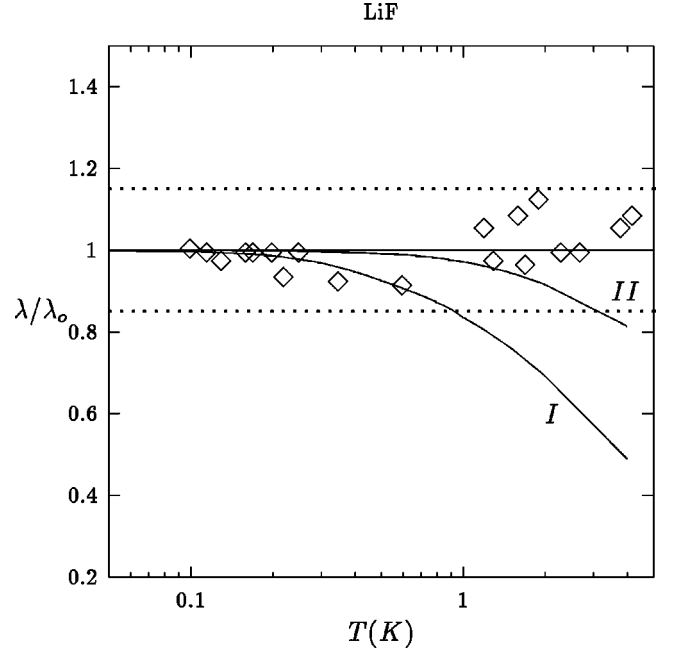


FIG. 2. Ratio of the thermal conductivities of LiF in the sheared region ( $\lambda$ ) and outside the sheared region ( $\lambda_o$ ). For curve I  $\lambda_o$  is provided by Eq. (35), while for curve II it accounts for the presence of a low-density distribution of very small angle grain boundaries. The data are from RA. The area delimited by the dotted lines defines the experimental uncertainties.

## VI. THERMAL CONDUCTIVITY BELOW 5 K

We will first apply the theory to LiF, for which RA<sup>2</sup> measured the thermal conductivity by an experimental arrangement in which the heat flow was normal to a set of parallel grain boundaries produced by deformation (shearing) of the sample. In this case the sum over  $\sigma$  required by Eq. (21) is represented by only one term, corresponding to the above set. We take  $z$  as the axis of the heat flow, and  $[y, x]$  as the dislocation array by which we simulate each grain boundary of the set. Such a choice corresponds to saving only the term with  $\sigma = 5$  in Eq. (21). For LiF we use the following data from Srivastava:<sup>26</sup>  $s_L = 5.6 \times 10^5$  cm/s;  $s_T = 3.36 \times 10^5$  cm/s;  $\gamma = 1.2$ , and consequently from Eq. (22) of Ref. 22,  $\epsilon = 14.69$ . RA give 7000 Å as the separation between etch pits in the boundaries, and  $2 \times 10^{-2}^\circ$  as the corresponding misfit angle. From this information a Burger vector  $b \approx 2.4$  Å is deduced. The average separation between adjacent grain boundaries of the set ( $\sim 4 \times 10^{-3}$  cm according to RA), corresponds to a density  $\mathcal{N}$  of about  $250 \text{ cm}^{-1}$ . We note that the value of the misfit angle widely satisfies condition (34) (in this case  $\theta \gg b/L_x$ ) because the length of the specimen along the direction normal to the heat flow was 0.5 cm, so that  $b/L_x \approx 4.8 \times 10^{-8}$ , while  $\theta \approx 3 \times 10^{-4}$  rad. The Casimir length  $\mathcal{L}$  due to boundary scattering is chosen consistently with the value of 0.089 W/cm K<sup>4</sup> for the low-temperature limit of  $\lambda T^{-3}$  in the perfect crystal (see the experimental points given by RA<sup>2</sup>). From Eq. (35) one deduces  $\mathcal{L} = 0.36$  cm, which is consistent with the size of the sample used by RA (0.5 cm).

In Fig. 2 we plot the ratio  $\lambda/\lambda_o$ , where  $\lambda = \lambda_{zz}$  and  $\lambda_o$  is the thermal conductivity of the unstrained sample: if this is considered as a perfect lattice,  $\lambda_o$  must be represented by Eq.



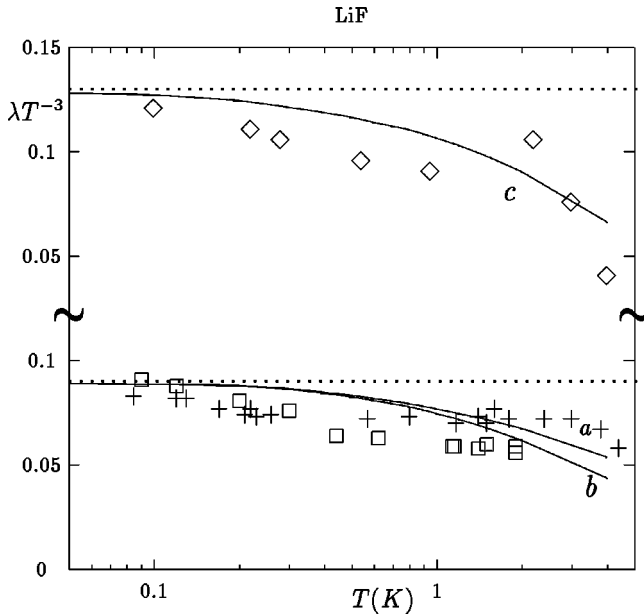


FIG. 3. Thermal conductivity of LiF divided by  $T^3$ , in units of  $\text{W/cm K}^4$ . The dotted lines represent the Casimir limit: the upper and the lower part of the figure refer to different sources of data (Refs. 27 and 2, respectively). Curves *a* and *c* represent the theoretical conductivity for an unstrained sample with a low-density distribution of very small angle grain boundaries, curve *b* accounts for a superimposed shear. All the experimental points refer to unstrained crystals, and + and  $\square$  to different samples used by RA.

(35) and the corresponding behavior of  $\lambda/\lambda_o$  is shown by curve I. Also shown are the experimental points of  $\lambda/\lambda_o$ , as deduced by RA for the sheared region. The points corresponding to  $\lambda/\lambda_o > 1$  are simply a measure of the uncertainty affecting the data: since a deformation of the sample cannot result in an increase of conductivity, one necessarily infers that each value of  $\lambda/\lambda_o$  is determined by an uncertainty of at least  $\pm 15\%$ , corresponding to the region between the dotted lines in the figure. The right conclusion of RA was that all the experimental points are indistinguishable from unity, so that the effect of shearing is negligible up to about 4 K. Now curve I is in agreement with this conclusion below 1 K: for higher temperatures, according to this curve the effect should be appreciable.

The reason of the discrepancy is that Eq. (35) was assumed to describe the conductivity of the unstrained region: this is not true, because the observed behavior of  $\lambda T^{-3}$  in this region is represented according to RA by the experimental points in the lower part of Fig. 3, which show a marked deviation from the Casimir limit (corresponding to the dotted line). The same behavior is confirmed by the measurements performed by In Sang Yang *et al.*<sup>27</sup> on an undeformed crystal of LiF (upper part of Fig. 3).

The present theory suggests a simple explanation of this behavior in terms of very low-angle grain boundaries, that we can assume to be present in any sample, even if not intentionally deformed. In this case, if no preferential direction exists in the sample, the model with the six dislocation walls (16) seems to be the most appropriate for a calculation of  $\lambda$ . In the frame of this model, for  $\theta \approx 10^{-3^\circ} - 10^{-4^\circ}$ , we require a linear density  $\mathcal{N}$  of only  $\sim 50 \text{ cm}^{-1}$  to explain the decrease of  $\lambda T^{-3}$  consistent with the data of RA for the

unstrained region (the result is almost independent of the choice of  $\theta$  since, as previously said, the theory predicts a saturation of the thermal resistance when  $\theta$  is very small). The theoretical behavior of  $\lambda T^{-3}$  between 0 and 4 K for  $\mathcal{N} = 50 \text{ cm}^{-1}$  is shown by curve (a) of Fig. 3.

In the frame of this model, we can refine our previous theory of thermal conductivity in deformed samples of LiF. The effect of deformation results in a set of parallel grain boundaries with density  $\mathcal{N}' \approx 250 \text{ cm}^{-1}$  [characterized by  $\sigma = 5$  in Eq. (21)] which is now added to the six sets of dislocation arrays pre-existing in the undeformed sample (with  $\mathcal{N} \approx 50 \text{ cm}^{-1}$ ). To treat this system, we have simply to put  $\mathcal{N} \approx 50 \text{ cm}^{-1}$  in Eqs. (20)–(22) and add to the first term on the RHS of Eq. (21) (evaluated for  $\theta = 10^{-3^\circ} - 10^{-4^\circ}$ ) the contribution corresponding to  $\sigma = 5$ ,  $\theta = 2 \times 10^{-2^\circ}$ , multiplied by  $\mathcal{N}'/\mathcal{N}$ . The resulting behavior of  $\lambda T^{-3}$  is represented by curve (b) of Fig. 3. The difference between the theoretical curves (a) and (b), referring to the undeformed and deformed regions, respectively, is within the uncertainties affecting the measurements of  $\lambda$ , as shown by the scattering of experimental points for the undeformed sample. This amounts to saying that the effect of deformation is negligible up to  $\sim 4 \text{ K}$ , in full agreement with the conclusions of RA. In fact the ratio between curve (a) and (b), as represented by curve II of Fig. 2, is essentially confined to the region between the dotted lines up to 3 K, and not significantly out of this region at 4 K.

We also analyzed the data of In Sang Yang *et al.* in terms of an assumed distribution of grain boundaries with  $\theta \approx 10^{-3^\circ} - 10^{-4^\circ}$ . Taking a Casimir length of 0.46 cm (consistent with the experimental limit of  $\lambda T^{-3}$ ) and a linear density of about  $80 \text{ cm}^{-1}$  we found curve *c* of Fig. 3, which shows a satisfactory fit to the experimental points. These conclusions are in full agreement with our previous analysis of RA data: the discrepancy between the values of  $\mathcal{N}$  related to curves *a* and *c*, respectively, is simply a consequence of the different samples to which they refer.

At this point we are in a position to discuss the weight of the processes considered by the Klemens theory: if the terms with  $n=0$  in Eq. (21) are omitted, the points of curve *b* of Fig. 3 are lowered by less than 1.5% at 0.1 K and by less than 1% at 0.5 K. This confirms that when the grain boundary density is low, the role of the above processes is negligible even for  $T \rightarrow 0$ , in which limit  $\lambda$  is essentially determined by Casimir length.

## VII. THERMAL CONDUCTIVITY IN THE PEAK REGION

A strong support to the above model comes from the analysis of the conductivity data obtained by Thacher<sup>28</sup> for monocrystals of LiF in the range between 1 and 100 K (see Fig. 4). To discuss the behavior of  $\lambda$  in this range we need to introduce umklapp three-phonon processes. Following Klemens,<sup>29</sup> p. 50, one can approximately describe these processes through a relaxation time

$$\frac{1}{\tau_U} = \nu_o \frac{\hbar \omega_p}{k_B T} e^{-\Theta_D/\alpha T}, \quad (36)$$

where  $\Theta_D$  is the Debye temperature,  $\alpha$  a dimensionless parameter of the order of 2, and  $\nu_o$  a characteristic frequency.

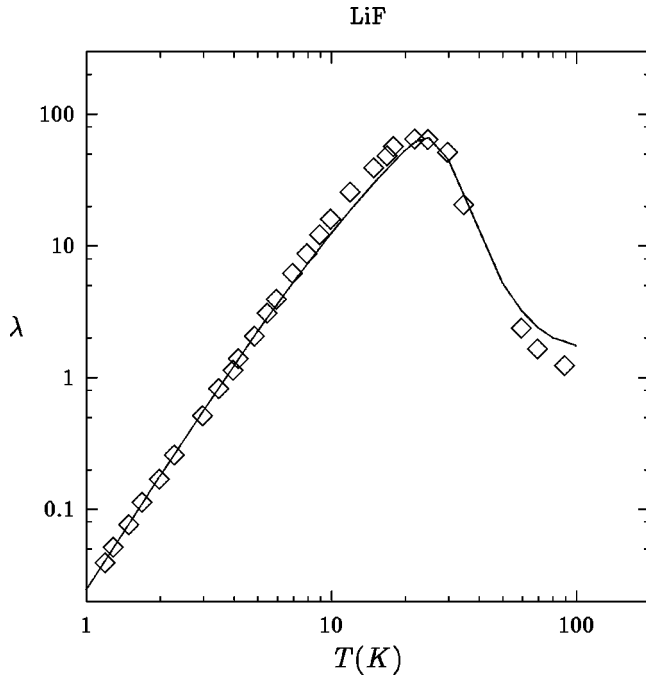


FIG. 4. Thermal conductivity of LiF in units of W/cm K as a function of temperature. The data are from Thacher (Ref. 28). The agreement with experimental data is obtained by introducing a low-density distribution of very small angle grain boundaries.

If very low angle grain boundaries are present in the crystal, as suggested in Sec. VI, they are expected to contribute in a significant way to the conductivity peak. Let us see if the form of this peak can be reproduced through a reasonable choice of the parameters  $\mathcal{N}$  and  $\nu_o$ . To this purpose, we point out that the total relaxation time  $\tau$  due to boundary scattering and umklapp processes is given by the relation  $1/\tau = 1/\tau_U + s_p/\mathcal{L}$ : this amounts to substituting Eq. (22) by the expression  $[1 + \mathcal{K} \exp(-\Theta_D/\alpha T)]\rho$ , where  $\mathcal{K} = \nu_o \mathcal{L}/s_T$ . After this substitution we can solve Eq. (21) and calculate the conductivity, as resulting from the simultaneous effects of boundary, grain boundary and umklapp scattering processes. We obtain the continuous curve of Fig. 4, which shows a good fit to the experimental points. The curve was deduced by taking  $\alpha = 2$ ,  $\mathcal{K} = 1.1 \times 10^5$ ,  $\theta \approx 10^{-3} - 10^{-4}$ ,  $\mathcal{N} = 80 \text{ cm}^{-1}$ ,  $\Theta_D = 620 \text{ K}$ ,<sup>29</sup> and a Casimir length of 0.095 cm: this follows from the experimental value of the left-hand side of Eq. (35) and is consistent with the size of the specimen used by Thacher ( $1.23 \times 0.91 \text{ mm}$ ). The relevant result is represented by the value of  $\mathcal{N}$ , which is comparable to the grain boundary density previously obtained from the analysis of the region below 5 K. This means that the assumption of a low density distribution of very small angle grain boundaries is sufficient to explain the observed behavior between 0.1 and 100 K, where  $\lambda$  changes by about six orders of magnitude.

The characteristic frequency  $\nu_o$  follows from the values obtained for  $\mathcal{K}$  and  $\mathcal{L}$ . One finds  $\nu_o \sim 5 \times 10^{11} \text{ s}^{-1}$ . To show that this is of the expected order of magnitude, one can in principle express in terms of Eq. (36) the thermal conductivity for an unbounded perfect crystal of the same material: the relation is

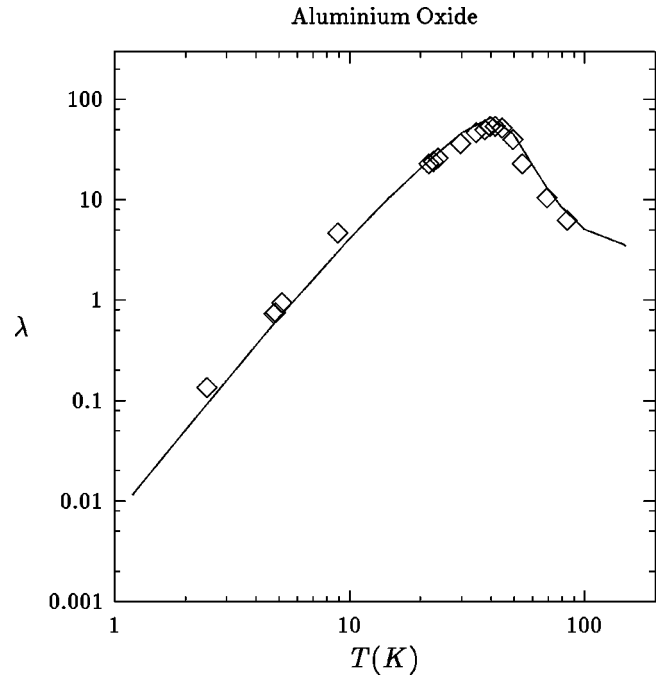


FIG. 5. Thermal conductivity of aluminum oxide in units of W/cm K as a function of temperature. The data are from Berman (Ref. 6). As for LiF the continuous curve accounts for the presence of a low density distribution of very small angle grain boundaries.

$$\lambda_\infty = 0.36 \frac{k_B^4 T^3}{\nu_o s \hbar^3} e^{\Theta_D/\alpha T}, \quad (37)$$

where  $s$  is an average sound velocity and the subscript  $\infty$  refers to the Casimir length, which in this case is infinitely large. If  $\lambda_\infty$  is independently known, the above relation can be used to obtain  $\nu_o$ . Unfortunately, there is no information on  $\lambda_\infty$  for LiF. However, as suggested by Eq. (9.4) of Ref. 29, it is reasonable to assume that the order of magnitude of  $\nu_o$  is the same for all solids: in this way we can refer to solid Argon, for which  $\lambda_\infty$  has been determined through a rigorous numerical solution of the transport equation:<sup>18</sup> at 20 K, one has  $\lambda_\infty = 16.6 \text{ mW/cm K}$ . Putting  $\alpha = 2$ ,  $\Theta_D = 80 \text{ K}$ ,  $s = k_B \Theta_D / \hbar Q \sim 0.94 \times 10^5 \text{ cm s}^{-1}$ , one readily obtains for this solid  $\nu_o \sim 4.95 \times 10^{11} \text{ s}^{-1}$ , which is about the same value as that previously obtained for LiF. The consistency of these two results represents a strong support to the validity of the proposed model.

The same model can successfully be applied to other materials. In Figs. 5 and 6 we show the remarkable agreement between the experimental points and the theoretical curves for alumina and quartz, respectively. The data of Fig. 5 are from Berman,<sup>6</sup> while the continuous curve has been deduced through the following choice of parameters:  $\alpha = 2$ ,  $\mathcal{K} = 0.5 \times 10^5$ ,  $\mathcal{N} = 60 \text{ cm}^{-1}$ ,  $\theta \approx 10^{-3} - 10^{-4}$ ,  $\mathcal{L} = 0.14 \text{ cm}$ ,  $\Theta_D = 980 \text{ K}$ ,  $s_L = 9.96 \times 10^5 \text{ cm s}^{-1}$ ,  $s_T = 5.95 \times 10^5 \text{ cm s}^{-1}$ ,  $b = 2.06 \text{ Å}$ ,  $\gamma = 3$  (corresponding to  $\epsilon = 24$ ). The data for quartz, to which the upper part of Fig. 6 is referred, are from Zeller and Pohl<sup>9</sup> and curve (a) was obtained by choosing  $\alpha = 2$ ,  $\mathcal{K} = 0.5 \times 10^5$ ,  $\mathcal{N} = 50 \text{ cm}^{-1}$ ,  $\theta \approx 10^{-3} - 10^{-4}$ ,  $\mathcal{L} = 0.5 \text{ cm}$ ,  $\Theta_D = 290 \text{ K}$ ,  $s_L = 5.97 \times 10^5 \text{ cm s}^{-1}$ ,  $s_T = 3.76 \times 10^5 \text{ cm s}^{-1}$ ,  $b = 3.3 \text{ Å}$ ,  $\gamma = 0.7$  (corresponding to  $\epsilon = 13.5$ ). The Debye temperatures and the Grüneisen con-

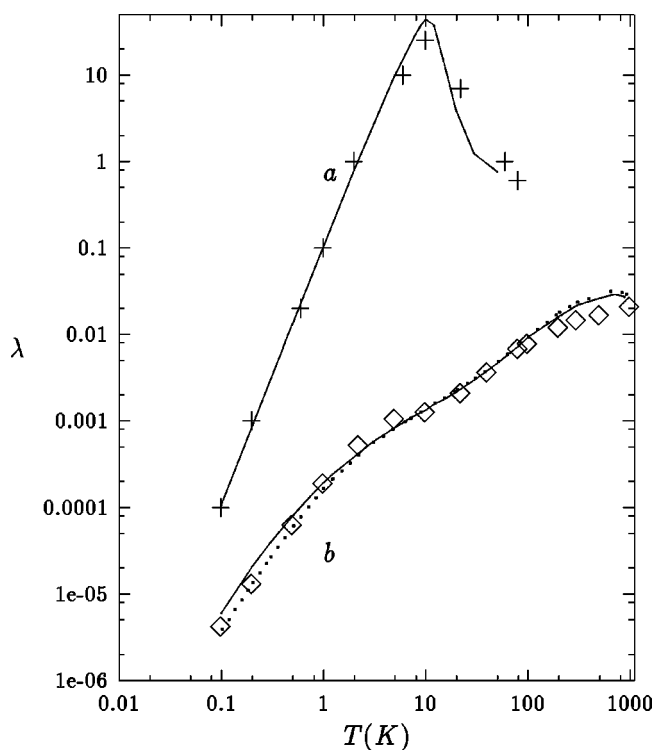


FIG. 6. Thermal conductivity of quartz (+) and of fused silica (◇) in units of W/cm K as a function of temperature. The data are from Ref. 9. The corresponding theoretical curves *a* and *b* account for the presence of small angle grain boundaries, with low density in the crystal and high density in the vitreous state.

stants are from Klemens<sup>29</sup> (p. 47), the sound velocities for alumina have been deduced from the values of Young modulus and bulk modulus as given by Ref. 30 for (isotropic) quartz from the corresponding velocities of fused silica;<sup>31</sup> the Casimir lengths follow from the experimental value of the LHS of Eq. (35) and turn out to be in good agreement with the sizes of the crystals used in Refs. 6 and 9 (1.5 mm and 5 mm, respectively); finally the Burger vectors have been approximately represented by  $\mathcal{V}^{1/3}$ , where  $\mathcal{V}$  is the average volume per atom as given by Klemens<sup>29</sup> (p. 47). The values obtained for  $\mathcal{N}$  show that a distribution of very small angle grain boundaries emerges as the plausible origin of the observed behavior of both the crystals, in full agreement with our previous result on LiF.

### VIII. AMORPHOUS DIELECTRIC SOLIDS

As a final application of the theory, we present in this section a model for amorphous solids which, in spite of its simplicity, is helpful to understand some unexplained features of the thermal conductivity curves of glasses. We will simply picture a glass as a crystal containing a high density distribution of grain boundaries. This picture is justified by the works of Kauzmann<sup>32</sup> and Phillips,<sup>33</sup> who described a glass as an assembly of small crystalline grains (microclusters with average diameter of order of 20–30 Å): in fact the parallelepiped cells resulting from the intersections of the three orthogonal sets of grain boundaries generated by Eq. (41) (that is, with planes normal to *x*, to *y* and to *z*, respectively) can be precisely interpreted as the microcrystals of

Refs. 32,33, provided the average distance between two adjacent grain boundaries of the same set is of the above order of magnitude.

In the spirit of this model, we will regard fused silica as a quartz lattice perturbed by a high density distribution of grain boundaries. Therefore the value of  $\nu_o$  is fixed, being precisely the one corresponding to quartz. Let us first suppose that the only source of thermal resistance is represented by boundary and grain boundary scattering. We can write  $\mathcal{K} = \mathcal{K}_o \mathcal{L} / \mathcal{L}_o$ , where  $\mathcal{K}$  and  $\mathcal{L}$  refer to fused silica, and  $\mathcal{K}_o$ ,  $\mathcal{L}_o$  to quartz. Since also  $\mathcal{L}$  is fixed (by the size of the specimen, in this case 0.5 cm, see Sec. V), we are left with two free parameters, namely,  $\mathcal{N}$ ,  $\theta$ , which can be varied so as to obtain the best fit of the theoretical curve to the experimental points, as determined by Zeller and Pohl. The results of our numerical analysis (to which the continuous curve *b* of Fig. 6 is referred) are  $\theta = 0.05^\circ$ ,  $\mathcal{N} = 6 \times 10^6 \text{ cm}^{-1}$ . The striking result is the numerical value of  $\mathcal{N}$ , corresponding to an average distance between grain boundaries of about 17 Å: this is comparable to the size of microcrystals predicted by Refs. 32,33. The small value of  $\theta$  means that the transition from a microcrystal to the neighboring one is smooth. With such a high density of grain boundaries,  $n=0$  processes play an important role in the low temperature limit. However, their contribution to the thermal resistance is progressively reduced as the temperature rises: it turns out to be 35%, 15%, and 2% of the total resistance at 1, 5, and 20 K, respectively, and becomes negligible at high temperatures.

It is important to emphasize that the theoretical behavior is almost unaffected by the value of  $\mathcal{K}_o$ . Changing  $\mathcal{K}_o$  by a factor 10 would not appreciably alter curve *b* of Fig. 6. This is quite reasonable, as  $\mathcal{K}_o$  is a parameter related to the presence of umklapp processes, which are not expected to play a role in an amorphous solid. When the density of grain boundaries is very high, there is no memory of the crystal order, and therefore of *U* processes which are a consequence of this order.

For pure quartz the theory could not be seriously applied to the temperature range beyond the peak, owing to the fact that our description of *U* processes, as based on Eq. (36), is reliable only at low temperatures: since, on the contrary, the conductivity of amorphous solids is essentially independent of these processes, we can approximately extend the theoretical curve up to temperatures of the order of 1000 K, where the experimental behavior presents a plateau. The relevant result is that the presence of this plateau is an automatic consequence of the theory, and is associated to the cutoff imposed to phonon wave vectors by the Debye radius *Q*: in fact, for  $Q \rightarrow \infty$  [that is, for  $\Theta \rightarrow \infty$  in Eq. (30)], one would obtain a monotonic increase of  $\lambda$  with temperature (not shown in Fig. 6).

Not all the features of the experimental curve are explained by the simple model we have presented. For instance, the plateau at ~10 K, which is systematically observed in all the amorphous solids, turns out to be substituted in curve *b* by a flex point at about the same temperature. This means that the model is not fully adequate, but has anyway to be considered as a good starting point for more refined calculations. At such a conclusion we also arrive through the following argument.

In the range between 0.1 and 1 K the continuous curve *b*

is approximately represented by a power law of the form  $\lambda = A T^n$ , with  $A = 1.5 \times 10^{-4}$  and  $n \sim 1.4$ . Thus the theoretical temperature dependence is weaker than the quadratic dependence predicted by the TLS model ( $\lambda \propto T^2$ ). Such a result is not trivial, because the experimental data, as obtained by Zeller and Pohl<sup>9</sup> for a variety of vitreous materials, show that the most reliable value of  $n$  is lower than 2. The value resulting from our model satisfies this condition, although it is slightly lower than the value recommended by the above authors ( $\sim 1.8$ ). But this implies that the experimental slope can be fully explained if one superimposes to boundary and grain boundary scattering the scattering due to localized two level states. The presence of TLS scattering can be simply introduced into Eq. (15) by the formula  $\tau_{qp}^{-1} = (\tau_{qp})_{BS}^{-1} + (\tau_{qp})_{TLS}^{-1}$ , where  $BS$  refers to boundary scattering, while, according to Ref. 14, one can write

$$(\tau_{qp})_{TLS} = C \omega_{qp}^{-1}, \quad (38)$$

where  $C$  is a constant independent of  $T$ . The above formula for  $\tau_{qp}$  corresponds to multiplying expression (22) by  $1 + \mathcal{L}q/C = 1 + (\mathcal{L}k_B T / C \hbar s_T) t$ . At this point there is no difficulty to find the set of parameters  $\mathcal{N}, \theta, C$  for which the theoretical curve presents the best fit to the experimental points in the whole temperature range, and simultaneously reproduces the observed slope between 0.1 and 1 K. The result is  $\mathcal{N} = 5 \times 10^6 \text{ cm}^{-1}$ ,  $\theta = 0.05^\circ$ ,  $C = 5.9 \times 10^3$ . We note that in this way the average distance between grain boundaries is  $\mathcal{N}^{-1} \sim 20 \text{ \AA}$ , in full agreement with the expected size of microcrystals.<sup>32,33</sup> The corresponding curve is dotted in Fig. 6, and becomes undistinguishable from the continuous curve for  $T > 1 \text{ K}$ . We also note that part of the thermal resistance is accounted for by grain boundary scattering, so that the relaxation time attributed to TLS scattering is expected to be larger in our model than in previous calculations. This is confirmed by the numerical value obtained for  $C$ : owing to Eq. (38), it corresponds to a phonon mean free path  $l \sim 940 \lambda_{ph}$ , where  $\lambda_{ph}$  is the phonon wavelength. Such a value of  $l$  is about 6 times larger than the value deducible from the data between 0.1 and 1 K if these are interpreted in terms of TLS scattering alone: in fact in this case the empirical relation is<sup>14</sup>

$$l \sim 150 \lambda_{ph}. \quad (39)$$

To show that the above result is quantitatively in agreement with the theoretical basis of the TLS model, we recall that this model predicts  $l/\lambda_{ph} \propto 1/\gamma^2$ , where  $\gamma$  is the phonon-TLS coupling constant. It has been pointed out by Karpov and Parshin<sup>12</sup> that a reasonable value for  $\gamma$  should be of the order of  $\sim 0.3 \text{ eV}$ , while the value ( $\gamma_o$ ) resulting from an empirical relation similar to Eq. (39) is considerably higher ( $\sim 1 \text{ eV}$ ). If one accepts the present model, the value of  $\gamma$  is reduced to  $(150/940)^{1/2} \gamma_o \sim 0.4 \text{ eV}$ , which is close to the theoretical estimate.

The model could be improved by the inclusion of Rayleigh scattering,<sup>34</sup> phonon assisted fracton hopping,<sup>16,17</sup> resonance scattering of thermal phonons by anharmonic oscillators.<sup>12</sup> A plausible result of this program would be the renormalization of all the constants entering the description of the above processes: as in the case of the phonon-TLS coupling constant, such a renormalization could be helpful for a better understanding of the processes themselves.

TABLE II. Components of tensor  $T_{ij}^{kl}$  in terms of the quantities defined by Eqs. (A1)–(A9).

$ij \backslash kl$	11	12	13	22	23	33
11	$3g_5$	$3a$	$3b$	$d$	$c$	$e$
12	$3a$	$d$	$c$	$3a$	$b$	$a$
13	$3b$	$c$	$e$	$b$	$a$	$b$
22	$d$	$3a$	$b$	$3h_5$	$3c$	$f$
23	$c$	$b$	$a$	$3c$	$f$	$3c$
33	$e$	$a$	$3b$	$f$	$3c$	$3l_5$

A final comment concerns the absence of optical phonons. This can be justified at any temperature for which the conductivity in fused silica is much lower than in quartz: in fact in this case all the scattering mechanisms responsible for the resistance in the perfect crystal (including scattering by optical phonons) are expected to be negligible with respect to grain boundary scattering, which is the main source of thermal resistance in the vitreous state. By inspection of the curve given in Ref. 9, one deduces that the above condition is only approximately verified at high temperatures, where the conductivity in fused silica is only one order of magnitude lower than in quartz. For such high temperatures, therefore, the inclusion of optical modes would represent a necessary improvement of the model.

## APPENDIX

The tensors  $T_{ij}^{kl}$  and  $M_{kl}$  are defined in terms of the quantities

$$a = \sin \theta \sin \theta' \sin(\phi + \phi'), \quad (A1)$$

$$b = \sin \theta \cos \phi \cos \theta' + \cos \theta \sin \theta' \cos \phi', \quad (A2)$$

$$c = \sin \theta \sin \phi \cos \theta' + \cos \theta \sin \theta' \sin \phi', \quad (A3)$$

$$d = 3 \sin \theta \sin \theta' \cos(\phi - \phi') + \cos \theta \cos \theta', \quad (A4)$$

$$e = \sin \theta \sin \theta' (3 \cos \phi \cos \phi' + \sin \phi \sin \phi') + 3 \cos \theta \cos \theta', \quad (A5)$$

$$f = \sin \theta \sin \theta' (\cos \phi \cos \phi' + 3 \sin \phi \sin \phi') + 3 \cos \theta \cos \theta', \quad (A6)$$

$$g_n = \sin \theta \sin \theta' (n \cos \phi \cos \phi' + \sin \phi \sin \phi') + \cos \theta \cos \theta', \quad (A7)$$

$$h_n = \sin \theta \sin \theta' (\cos \phi \cos \phi' + n \sin \phi \sin \phi') + \cos \theta \cos \theta', \quad (A8)$$

$$l_n = \sin \theta \sin \theta' \cos(\phi - \phi') + n \cos \theta \cos \theta'. \quad (A9)$$

$T_{ij}^{kl}$  is symmetric with respect to the exchanges  $i \leftrightarrow j$  and  $k \leftrightarrow l$  and is provided by Table II. The tensor  $M_{ik}$  is also symmetric and its components are  $M_{11} = g_3$ ,  $M_{12} = a$ ,  $M_{13} = b$ ,  $M_{22} = h_3$ ,  $M_{23} = c$ ,  $M_{33} = l_3$ .



- <sup>1</sup>P.G. Klemens, Proc. Phys. Soc. London **68**, 1113 (1955).  
<sup>2</sup>E.P. Roth and A.C. Anderson, Phys. Rev. B **17**, 3356 (1978).  
<sup>3</sup>S.E. Krasavin and V.A. Osipov, Phys. Lett. A **236**, 245 (1997).  
<sup>4</sup>(a) J.M. Ziman, *Electrons and Phonons* (Claredon Press, London, 1962), p. 229; (b) *ibid.*, p. 325.  
<sup>5</sup>A.C. Anderson and M.E. Malinowski, Phys. Rev. B **5**, 3199 (1972).  
<sup>6</sup>R. Berman, Proc. Phys. Soc. London **65**, 1029 (1952).  
<sup>7</sup>P.G. Klemens, Proc. R. Soc. London, Ser. A **208**, 108 (1951).  
<sup>8</sup>P.G. Klemens, in *Physics of Non-crystalline Solids*, edited by J.A. Prins (North-Holland, Amsterdam, 1965), p. 162.  
<sup>9</sup>R.C. Zeller and R.O. Pohl, Phys. Rev. B **4**, 2029 (1971).  
<sup>10</sup>P.W. Anderson, B.I. Halperin, and C.M. Varma, Philos. Mag. **25**, 1 (1972).  
<sup>11</sup>W.A. Phillips, J. Low Temp. Phys. **7**, 351 (1972).  
<sup>12</sup>V.G. Karpov and D.A. Parshin, Zh. Éksp. Teor. Fiz. **88**, 2212 (1985) [Sov. Phys. JETP **61**, 1308 (1985)].  
<sup>13</sup>Yu.M. Galperin, V.G. Karpov, and V.I. Kozub, Adv. Phys. **38**, 669 (1989).  
<sup>14</sup>J.J. Freeman and C. Anderson, Phys. Rev. B **34**, 5684 (1986).  
<sup>15</sup>S. Alexander, O. Entin-Wohlman, and R. Orbach, Phys. Rev. B **34**, 2726 (1986).  
<sup>16</sup>A. Jagannathan, R. Orbach, and O. Entin-Wohlman, Phys. Rev. B **39**, 13 465 (1989).  
<sup>17</sup>R. Orbach, Philos. Mag. B **65**, 289 (1992).  
<sup>18</sup>M. Omini and A. Sparavigna, Phys. Rev. B **53**, 9064 (1996).  
<sup>19</sup>M. Omini and A. Sparavigna, Nuovo Cimento D **19**, 1537 (1997).  
<sup>20</sup>M. Omini and G. Teppati, Nuovo Cimento D **8**, 597 (1986).  
<sup>21</sup>G.P. Srivastava, *The Physics of Phonons* (Adam Hilger, Bristol, 1990).  
<sup>22</sup>F. Iazzi, M. Omini, Nuovo Cimento D **8**, 582 (1986).  
<sup>23</sup>J.P. Hirth and J. Lothe, *Theory of Dislocations* (John Wiley, New York, 1982), p. 732.  
<sup>24</sup>D.C. Wallace, *Thermodynamics of Crystals* (Wiley, New York, 1972), p. 178.  
<sup>25</sup>J. Callaway, Phys. Rev. **113**, 1046 (1959).  
<sup>26</sup>G.P. Srivastava, J. Phys. Chem. Solids **41**, 357 (1980).  
<sup>27</sup>In Sang Yang, A.C. Anderson, Y.S. Kim, and E.J. Cotts, Phys. Rev. B **40**, 1297 (1989).  
<sup>28</sup>P.D. Thacher, Phys. Rev. **156**, 975 (1967).  
<sup>29</sup>P.G. Klemens, in *Solid State Physics*, edited by F. Seitz and D. Turnbull (Academic Press, New York, 1958), Vol. 7.  
<sup>30</sup>ALMAZ Optics Inc., West Berlin, NJ 08091, URL <http://www.vlproducts.com/>  
<sup>31</sup>*American Institute of Physics Handbook* (McGraw-Hill, New York, 1957), Sec. 3-80.  
<sup>32</sup>W. Kauzmann, Chem. Rev. **43**, 219 (1948).  
<sup>33</sup>J.C. Phillips, in *Solid State Physics*, edited by S.H. Ehrenreich and D. Turnbull (Academic Press, New York, 1983), Vol. 37, p. 93.  
<sup>34</sup>D.P. Jones, N. Thomas, W.A. Phillips, Philos. Mag. B **38**, 271 (1978).